Smart Structures and Systems, *Vol. 25, No. 5 (2020) 515-530*
DOI: https://doi.org/10.12989/sss.2020.25.5.515

Investigation on the performance of a new pure torsional yielding damper

Shahram Lotfi Mahyari [a], Hossein Tajmir Riahi* and Mahmoud Hashemi Esfahanian [b]

Department of Civil Engineering, Faculty of Civil Engineering & Transportation, University of Isfahan, Iran

(*Received May 5, 2019, Revised November 23, 2019, Accepted January 30, 2020*)

Abstract. A new type of pure torsional yielding damper made from steel pipe is proposed and introduced. The damper uses a special mechanism to apply force and therefore applies pure torsion in the damper. Uniform distribution of the shear stress caused by pure torsion resulting in widespread yielding along pipe and consequently dissipating a large amount of energy. The behavior of the damper is investigated analytically and the governing relations are derived. To examine the performance of the proposed damper, four types of the damper are experimentally tested. The results of the tests show the behavior of the system as stable and satisfactory. The behavior characteristics include initial stiffness, yielding load, yielding deformation, and dissipated energy in a cycle of hysteretic behavior. The tests results were compared with the numerical analysis and the derived analytical relations outputs. The comparison shows an acceptable and precise approximation by the analytical outputs for estimation of the proposed damper behavior. Therefore, the relations may be applied to design the braced frame system equipped by the pure torsional yielding damper. An analytical model based on analytical relationships was developed and verified. This model can be used to simulate cyclic behavior of the proposed damper in the dynamic analysis of the structures equipped with the proposed damper. A numerical study was conducted on the performance of an assumed frame with/without proposed damper. Dynamic analysis of the assumed frames for seven earthquake records demonstrate that, equipping moment-resisting frames with the proposed dampers decreases the maximum story drift of these frames with an average reduction of about 50%.

Keywords: yielding damper; pure torsion; finite element method; pipe; dissipated energy

1. Introduction

During earthquake, a large amount of energy is applied on the structure that should be either controlled or damped. The energy is normally damped by developing plastic hinges along the main elements of the seismic resisting system in the conventional structures. This increases the post-earthquake repair cost of the structure and makes the maintenance too expensive. During recent decades, the seismic control systems such as base isolators and dampers are widely developed and used to resolve the issue. In the dampers-equipped structures, new members are designed and constructed to absorb the seismic energy. The members make the behavior of the structure more desired and better and therefore the seismic performance of the structure is optimized. As a result, the post-earthquake repair cost of the structure is much more limited compared to the conventional structures.

The dampers used in the structures are categorized according to their energy damping mechanism into four groups as frictional, viscous, visco-elastic and yielding. The yielding dampers utilize the considerable energy absorbing capacity of metallic materials. Various force mechanisms are proposed to utilize the capacity by various researchers. A combination of internal forces is normally made by majority of the damping systems. Although the combination also exists in the current yielding systems, the yielding process is mainly governed by either of the bending, shear, axial or torsional elements. Usually the combination of different kind of forces throughout damper creates non-uniform stress and so non-uniform yielding which prevents the optimum use of the energy damping capacity of damper material.

Among the bending performance type of the dampers are those made from plates including ADAS (Whittaker *et al*. 1989), TADAS (Tsai *et al*. 1993, Gray *et al*. 2012), rhombic shape (Shih and Sung 2005), U-shape (Aguirre and Sanchez 1992, Tagawa and Gao 2012, Deng *et al*. 2013, 2015b), J-shape (Kato *et al*. 2005, Kato and Kim 2006), E-shape (Ciampi and Marioni 1991, Tsopelas and Constantinou 1997), pipe in pipe (Cheraghi and Zahrai 2017), pure bending (Zibasokhan *et al*. 2019), and Butterfly-Shaped (Farzampour *et al*. 2019), that are studied by various researchers. The shear force makes changes in bending moment inside the damper's plate. Therefore, the plate width is changed according to bending moment variations to make its curvature constant and cause widespread hinge.

The systems utilizing shear mechanism has the ability to completely absorb energy because of the simultaneous plasticity in shear. But most of the dampers using the shear mechanism may not be able to show their complete shear yielding capacity due to shear buckling. Many suggestions are made to postpone the shear buckling including vertical and horizontal stiffening plates (Nakashima *et al*. 1994),

*Corresponding author, Assistant Professor,
E-mail: tajmir@eng.ui.ac.ir
[a] Research Assistant, E-mail: shahram_lotfi86@yahoo.com
[b] Associate Professor, E-mail: m.hashemi@eng.ui.ac.ir

ISSN: 1738-1584 (Print), 1738-1991 (Online)

making vertical slits (Hitaka and Matsui 2003), making horizontal slits (Chan and Albermani 2008), making non-uniform slits (Lee *et al*. 2015), making hole in the plate (Chan *et al*. 2013), using circular plates (Abebe and Choi 2014), lateral bracing (Deng *et al*. 2015a) and elliptical-shaped (Zahrai and Mortezagholi 2017).

The buckling in compression forces becomes a problem in long elements of dampers which yield in axial force. This makes the difference between tensile and compressive capacity of the damper and yielding capacity of materials is not completely used in compressive force. The matter is resolved by adding lateral support (Black *et al*. 2004). Buckling restrained braces become popular in recent years and different efforts are made to enhance their performance (Benavent-Climent 2010, Piedrafita *et al*. 2013, 2015, Razavi *et al*. 2014).

Another category includes dampers making torsional-induced shear which may not face torsional buckling. Various cross sections are recommended by researchers such as rectangular (Skinner *et al*. 1975), circular (Franco *et al*. 2010, Milani and Dicleli 2016, 2017) and tubular (Vetr and Ghamari 2012). The current torsional moment-based dampers normally produce shear force due to exerting eccentric force to cause torsion in the damper section. The induced shear force makes the stress distribution non-uniform. Non-uniform stress distribution causes premature failure and prevents optimum use of energy dissipation capacity of materials in the existing dampers. Since a pure torsional moment-based damper is not introduced yet, a new pure torsion damper is introduced in this paper. In this damper, a special mechanism is used to convert story shear to pure torsion in the pipes. Hence, a uniform stress distribution is created in the wall of the pipes, which allows the energy absorbing capacity of the steel material to be used more efficiently.

2. The proposed torsional damper

A new torsion-based yielding damper (Fig. 1) is proposed which makes pure torsion in tubular element subjected to torsional moment. Application of the damper in a typical frame is shown in Fig. 2. The connection between damper device and frame is made by bolts for easy substitution of the damper after severe earthquake events. Ordinary holes are used in the bolt connection between damper device and inverted V brace whereas transverse slotted holes are used in the connection with story beam to prevent unexpected out of plane loading due to 2-D oscillations, as shown in Fig. 1. In fact, in-plane story shear is transferred to the damper device through the transverse slotted holes and out of plane relative movement between damper device and story beam is allowed without load transmission to the damper. The applied force at the story level, which makes inter-story drift, is converted into a couple of shear forces and finally produces pure torsion in the pipes (Fig. 1). The story-induced shear force is transferred to the handles connected to the pipes by a number of supports and links. The connection between handles, links and supports are made by bolted hinges. The bolts make the post-earthquake maintenance much easier and short-time. The supports are placed at the top and bottom in such a way that the force couple is applied simultaneously at the higher and lower handles connected to the pipe. In the opposite twin side of the damper, there are twin supports and the forces applied on the handles are of the same magnitude but in the opposite direction making a reverse pure torsional moment.

The links are used to connect handles to the top supports to prevent inducing axial force in handles during inter-story drift or story beam deformation under gravity loading. So, the handles are only subject to shear force and torsional moment produced by transfer of story shear to the pipes.

The damper may be used in chevron bracing (Fig. 2). This provides desired initial stiffness and lateral strength as well as the required ductility. Of course, the damping system may be simply fabricated and installed. Moreover, post-earthquake repair and maintenance is also a key advantage of the system. The diagonal elements of the bracing are to be connected to a horizontal rigid element located at the bottom of the damper (Fig. 2). Therefore, this chevron bracing may be considered as a concentric type of braced frame. Although the damper suitably matches chevron bracing frames but the damper can be used in the other types of bracings with little changes made in the damper geometry.

The damper not only has the advantage of making pure torsion but has other advantages such as carrying considerable lateral deformations, preventing transfer of gravity loads to the damper elements, low cost and simple technology of fabrication, availability of the damper materials, provision for fast replacement after severe earthquakes, thermal-independent behavior in conventional temperature, cheap maintenance and flexibility in design.

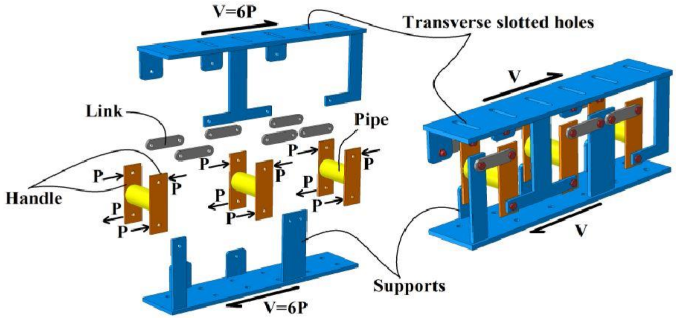

Fig. 1 The proposed damper details and its performance mechanism

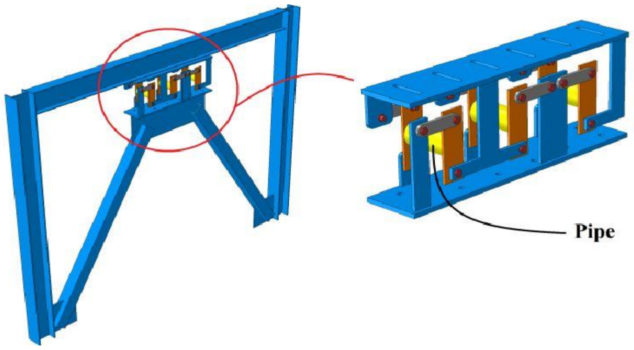

Fig. 2 The overall view of chevron bracing frame equipped with the proposed torsional damper

The structural characteristics of the damper (such as stiffness, strength, ductility and energy absorbing capacity) may be determined according to the selection of number and types of the pipes. Using the damper makes the conventional concentric braced frames more ductile. Together with the advantage of desired stiffness in the braced frames compared to moment-resisting frames and low cost of replacement and maintenance, the damper has many sufficient advantages for using in structural frames.

3. Analytical investigation of the damper performance

To study the behavior of the proposed tubular torsional damper, the stress-strain behaviour is assumed as ideal elastic-perfectly plastic. The behavior characteristics are determined using simple relations in strength of materials. The loading mechanism is shown in Fig. 3. A couple of (reverse) forces are applied on the $2R_0$-long handle. The handles in both opposite sides are welded to the pipe. To reduce stress concentration in the welding region of the pipes during torsion, the pipes might be passed among the perforated handle and welded at both sides of the handle using high-quality reliable welding. The inner and outer radius of the pipe is c_i and c_o respectively and its thickness is t. It is also assumed that the story shear V is distributed equally between n dampers and the damper shear is also divided equally on the two sides and each side equally on two supports, preserving the mechanism shown in Fig. 3. Based on equilibrium of the forces, torsion on the pipe (T) and loads acting on the handles (P') are related as

$$P' = \frac{T}{2R_0} \tag{1}$$

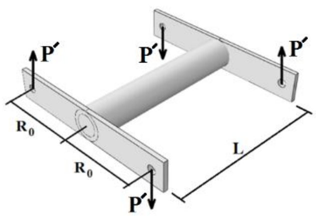

Fig. 3 Details of applying force and producing pure torsional moment in the damper

The pure torsional moment produced in the pipe, T, is calculated as sum of products of force P ($P = 2nP$') by handle arm for small deformations especially before yielding the damper whereas for large deformations, the rotation of pipe and the connected handle becomes more and therefore decreases the arm involved in the torsional moment applied to the pipes. Also, the assumption of ideal elastic-perfectly plastic means that the torsional moment tolerated by the pipe remains constant as the relative displacement applied to the damper increases. Considering above points, it may be concluded that with increase in the relative displacement applied to the damper, the shear force tolerated by the damper becomes more. Considering the damper geometry, the reductions in the effective arm are different in tensile and compressive zones. Therefore, the difference makes the different behavior for damper under tensile and compressive loadings (Fig. 4).

The angles and distances corresponding to the following relations are shown in Fig. 4. The φ denotes the relative rotation angle of two sides of the pipe whereas θ is equal to the rotation angle of either side of the tube with respect to the horizon. The unit less parameter j is defined as follows

$$j = \frac{\vec{\delta}}{|\delta|} \tag{2}$$

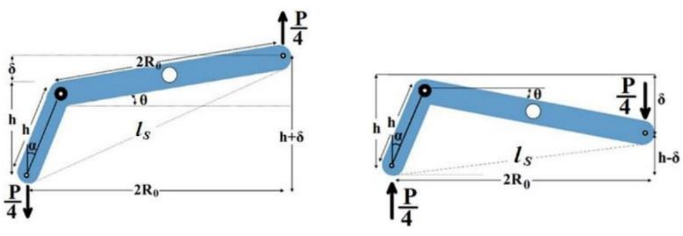

Fig. 4 Details of torsion of pipe handles in large deformations

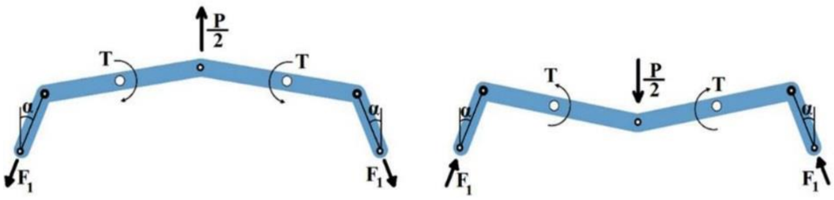

Fig. 5 Free body diagram of handles connected to the pipe in large deformations

Therefore, the *j* parameter always becomes unity and its sign is positive/negative in tensile/compressive deformations, respectively. The relation between torsional moment and shear force that can be tolerated by the pipe is derived by applying simple equilibrium (Fig. 5). The following relation may be expressed for large deformations as

$$l_s = \sqrt{(2R_0)^2 + (h + j\delta)^2} \tag{3}$$

$$\alpha = \frac{\pi}{2} - tan^{-1}(\frac{h + j\delta}{2R_0}) - cos^{-1}(\frac{h^2 + (h + j\delta)^2}{2hl_s}) \tag{4}$$

$$\theta = \frac{\phi}{2} = cos^{-1}(1 - \frac{h\sin\alpha}{2R_0}) \tag{5}$$

$$F_1 \cos\alpha = \frac{P}{2n} \tag{6}$$

$$T = F_1(2R_0)\cos(\alpha + j\frac{\phi}{2}) \tag{7}$$

$$P = \frac{2n}{2R_0} \times \frac{\cos\alpha}{\cos(\alpha + j\frac{\phi}{2})} \times T \tag{8}$$

where *P* is applied force tolerated to the damper in tensile/compressive; *n* is the number of pipes in each damper; F_1 is induced axial force in either links connected to the damper handles. It should be reminded that in small deformation, the reduction in the arm due to rotation used for torsional moment calculation may be ignored. Therefore, Eq. (1) can be used as an alternative to Eq. (8). Even in large deformations, Eq. (1) can be used instead of Eq. (8) with some approximation.

The details of producing shear stress due to torsional moment in tubular cross section is shown in Fig. 6. The yielding torsional moment of the tube (T_y) and the ultimate torsional moment of the pipe cross section (T_u) are derived according to this figure.

$$T_y = \int_0^{2\pi}\int_{c_i}^{c_o} \tau r^2 dr\, d\theta \tag{9}$$

$$\tau = \frac{r}{c_o}\tau_y \tag{10}$$

$$T_y = \int_0^{2\pi}\int_{c_i}^{c_o} \frac{r}{c_o}\tau_y r^2 dr\, d\theta = \frac{\pi\tau_y}{2c_o}(c_o^4 - c^4) \tag{11}$$

$$T_u = \int_0^{2\pi}\int_{c_i}^{c_o} \tau_y r^2 dr\, d\theta = \frac{2\pi\tau_y}{3}(c_o^3 - c^3) \tag{12}$$

Considering no large deformations, the force corresponding to the yielding (P_y), the corresponding ultimate force applied to the handles connected to the pipe (P_{u0}) and the relative rotation angle of two sides of the pipe in yielding (φ_y) and ultimate (φ_u) states can be expressed in the following form as

$$P_y = \frac{n\pi\tau_y(c_o^4 - c_i^4)}{2R_0 c_o} \tag{13}$$

$$P_{u0} = \frac{2n\pi\tau_y(c_o^3 - c_i^3)}{3R_0} \tag{14}$$

$$\phi_y = \frac{T_y L}{JG} \tag{15}$$

$$\phi_u = sin^{-1}(\frac{\delta_u}{R_0}) \tag{16}$$

$$J = \frac{\pi}{2}(c_0^4 - c_i^4) \tag{17}$$

where φ_u is ultimate rotation angle; φ_y is rotation angle corresponding to yield initiation; *J* is the polar moment of inertia for tubular cross section; *G* is shear modulus of pipe material; L is the pipe length and δ is relative lateral displacement of the stories.

Using the earlier relations, the yield rotation angle and initial stiffness of the damper are determined as

$$\phi_y = \frac{\pi\tau_y(c_o^4 - c_i^4)L}{2c_o\frac{\pi}{2}G(c_o^4 - c_i^4)} = \frac{L\tau_y}{c_0 G} \tag{18}$$

$$\delta_y = R_0 \sin(\frac{L\tau_y}{c_0 G}) \tag{19}$$

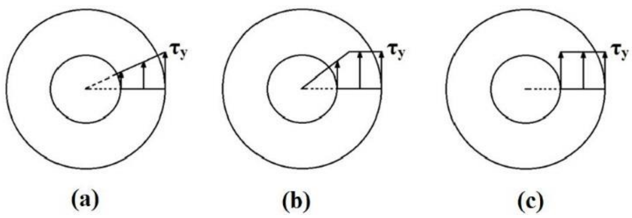

Fig. 6 Shear stress distribution in tubular cross section under (a) yielding torsional moment (T_y); (b) post-yielding torsional moment; (c) ultimate torsional moment (T_u)

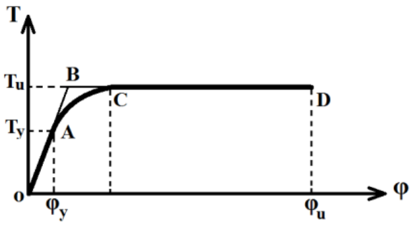

Fig. 7 Schematic torsional moment vs. rotation angle variations for the damper

$$K_i = \frac{P_y}{\delta_y} \tag{20}$$

Considering large deformation and Eq. (8), the ultimate force applied to the handles connected to the pipe (P_u) can be calculated as

$$P_u = \frac{2n\pi(c_o^3 - c_i^3)\tau_y}{3R_0} \times \frac{\cos\alpha}{\cos(\alpha + j\frac{\phi}{2})} \tag{21}$$

The torsional moment vs. rotation angle variations along with the yielding and ultimate torsional moment and also the corresponding rotation angles are shown in Fig. 7.

The damper material has linear behavior in the 1st part (OA) and has perfectly plastic behavior in the 3rd part (CD) of the Fig. 7. In-between the 1st and 3rd parts (AC), as applied torsional moment increases, the fibers of the cross section (from farthest towards nearest to the center) becomes yielded due to induced shear stress. Finally, all of the fibers are yielded at point C and the tolerable torsional moment may not further increase as the rotation angle becomes more. The amount of energy required for elastic deformation during a quarter of loading/unloading cycle may be expressed as the area under the OA part. Using virtual work principle, the amount of damped energy in a cycle may be expressed as follows

$$E_{pl} = 4(W - E_{el}) = 4(P\delta - E_{el}) \tag{22}$$

$$E_{el} = \frac{{P_{u0}}^2}{2K_i} \tag{23}$$

where W is the external work done during a quarter of cycle; E_{el} is elastic energy required to make deformation corresponding to yielding limit during a quarter of cycle; E_{pl} is the damped energy during a quarter of loading/unloading cycle; and P is applied force.

The applying force mechanism assumes that the story shear force is divided between the n dampers pipes equally. Based on the assumptions, the maximum damper force (P_u), damped energy (E_{pl}) can be derived as follows

$$E_{pl} = 4(\delta_u P_{u0} - E_{el}) = 4\delta_u P_{u0} - 2\frac{{P_{u0}}^2}{K_i} \tag{24}$$

where δ_u is ultimate imposed displacement. Assuming the steel material and the von-Mises yield criterion for steel behavior in the above relations, the yield shear stress τ_y is determined from tensile yield stress F_y for steel as follows

$$\tau_y = \frac{F_y}{\sqrt{3}} \tag{25}$$

4. Comparison of analytical, numerical and experimental results

In order to confirm the analytical calculations and to identify the ambiguities and possible differences with the assumptions made, there is a need for a laboratory test of the performance of the proposed damper. In this section, four samples of the torsional damper have been tested and the results of the tests are compared with the results of analytical and numerical analysis.

4.1 Experimental results of the proposed damper

Based on the performance mechanism described in the previous sections, the performance of the frame equipped with the proposed damper is directly related to the performance of the damper. For this reason, to study the performance of the frame, it is possible to examine the performance of the damper under the twist without considering the frame. Therefore, pure torsional moment is applied to the pipes as shown in Fig. 3 by force couple. Applying force couple like this creates conditions similar to the way the force is applied to the torsional damper in Fig. 1. In this section, the behavior of the materials used in the damper was first examined, and then the results of four samples were investigated and described.

4.1.1 Behavior of the damper material

The performance of a ductile member greatly depends on the properties of its materials. Therefore, tensile testing is used to understand the behavior of steel used in the pipes. Pipes used in this study are steel pipes with external diameter of 13.4, 20.7, 31.0 and 42.1 mm (pipe 14, pipe 21, pipe 31 and pipe 42) and internal diameter of 8, 14.2, 24.7 and 36.2 mm, respectively. These four samples are from three different types of steel with different specifications. Pipe 14 is made of X60 steel, pipe 21 and pipe 31 are made of St44 steel and pipe 42 is made of St52 steel. X60 steel has greater yield stress and less ductility rather than St44 and St52 steel. Considering the diameter of the pipes, the tensile test has been performed on the whole cross section of the pipe 14 and standard tensile coupon of the other pipes. Stress-strain graphs for X60, St44 and St52 steels are shown in Fig. 8. Table 1 shows the values of the tensile yield and ultimate stresses and the tensile ultimate strain for these four different types of pipes.

4.1.2 Experimental program

To perform a pure torsion test on the damper specimens with the geometry shown in Fig. 1, a special test setup is used as shown in Fig. 9. The uniaxial force applied to the setup produces pure torsional moment on the pipes based on the symmetry of the setup. As shown in Fig. 9, two intermediate links are used for each pipe in order to prevent creation of axial force in the handles same as proposed

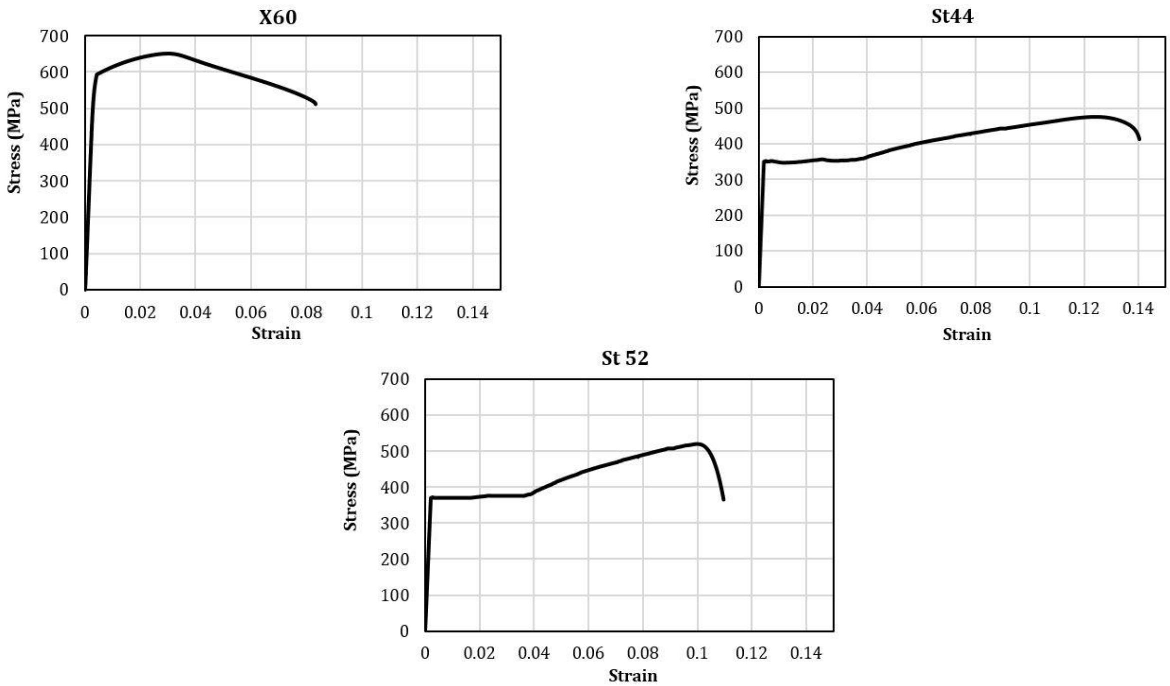

Fig. 8 Stress-strain behavior of the damper material

Table 1 Specification of the damper material

Pipe type	Steel type	Outer diameter (mm)	Inner diameter (mm)	Modulus of elasticity (GPa)	Yield stress (MPa)	Ultimate stress (MPa)	Strain at ultimate stress (%)	Rupture strain (%)
Pipe 14	X60	13.4	8	190	530	650	3	8.3
Pipe 21	St44	20.7	14.2	180	350	474	12.6	14
Pipe 31	St44	31	24.7	180	350	474	12.6	14
Pipe 42	St52	42.1	36.2	180	370	520	10	12.4

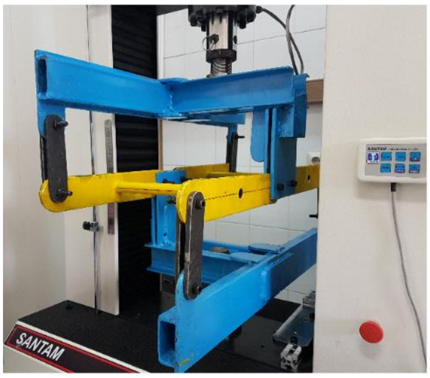

Fig. 9 Experimental test setup

damper in Fig. 1. One end of the link is connected to the handle while the other end is connected to the test setup using bolts to create pinned connection.

The length of the handle plays a significant role in the force and ductility capacity of the damper. Assuming a constant value for the torsional strength of the pipes, when the length of handle increases the force capacity of the damper decreases. Also, assuming a constant value for the torsional ductility of the pipes, the increase in the length of the handle leads to an increase in the displacement capacity of the damper and finally increases the ductility of the damper and structure equipped with it. This argument is justified by the relationships presented in Section 3.

The performance of the specimens during the test are shown in Figs. 10 and 11. In these figures, the deformation of the system and the pipes are shown when the applying force from the testing machine are tensile and compressive, respectively. The pipes were connected to the handles by use of welding as observable in Figs. 9-11. The pipes were passed through the holes made in the handles and welded on both sides of the handles to reduce stress concentration in the pipe at the connection point. The handle was reinforced at the connection point for specimens pipe 31 and 42, as visible in Fig. 11(b). Also, the handles of these specimens are reinforced by adding two plate as the flange of the handle to form an I-shape section to prevent lateral-torsional buckling in the handles during test, as observable in Figs. 10(b) and 11.

4.1.3 Experimental results

Among the existing loading protocols, ATC-24 and SAC protocols are widely used for steel structures (Piedrafita *et*

(a) Pipe 21 (b) Pipe 31

Fig. 10 Specimens pipe 21 and 31 at maximum tensile displacement

(a) Front view (b) Side view

Fig. 11 Specimen pipe 42 at maximum compressive displacement

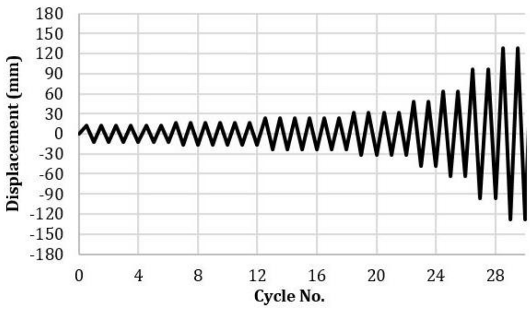

Fig. 12 The SAC loading protocol used in this study

Table 2 The SAC loading protocol used in this study

Inter-story drift ratio (%)	Number of cycles	Story displacement (mm)
0.375	6	12
0.5	6	16
0.75	6	24
1	4	32
1.5	2	48
2	2	64
3	2	96
4	2	128

al. 2013, 2015). ATC-24 loading protocol is based on the yielding deformation of the member while SAC loading protocol is based on the relative displacement between the stories of the building. In this paper, four diameters of pipes with different capacity have been tested and therefore their yielding deformations are different too. Finally, in order to compare the performance of these four specimens, SAC loading protocol is used which is independent of the yielding deformation and is the same for different specimens. Also, it is possible to assess the performance of the frames equipped with this type of damper with this protocol because it is based on inter-story drift. Fig. 12 shows the SAC loading protocol used in this study. This protocol is based on the height of the story assumed to be 3.2 meters.

Table 2 shows SAC loading protocol cycles and assumed drift variation in these cycles. A total number of 30 loading loops with a 4500 mm cumulative displacement are applied to the specimens in this loading protocol. The horizontal relative displacement of the story and the axial deformation of the damper are calculated based on a frame with a story height of 3.2 m and a span of 3.5 m. Loading speed of 250 mm/min is used for testing.

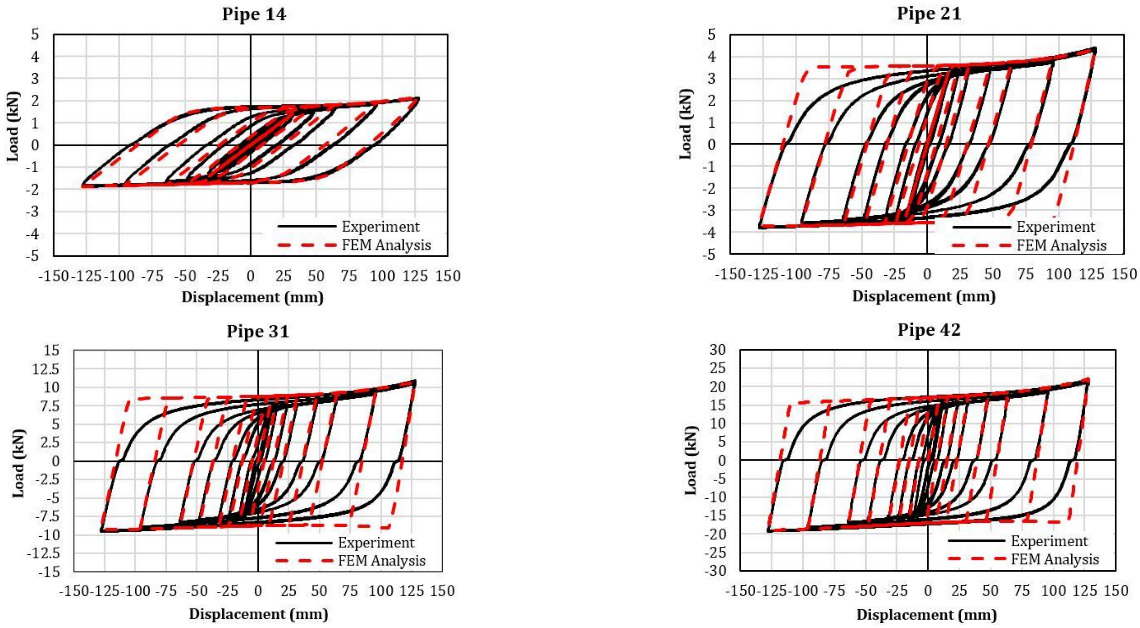

Fig. 13 Load-Displacement curves for specimens

Fig. 13 shows the load-displacement hysteretic behavior for the damper samples. In this figure, it can be seen that the proposed damper shows stable hysteresis cycles. Strain hardening of steel and gradually yielding of the pipe from outer surface to its inner surface increase damper strength after its first yield. Another reason for this increase is the change in the angle of the coupling force applied to the handles during loading, which increases with the increase of the deformation as shown in Fig. 4. In other words, by increasing the displacement in the test, the rotation of the pipe and the handle connected to it increases which reduces the effective arm of the torsion applied to the pipes. Torsional capacity of the pipe is constant and therefore this reduction will increase the shear force capacity that can be applied to the damper. Based on the geometry of the damper, this reduction in the effective arm in tensile and compressive forces varies, which causes differences in the behavior of the dampers under tensile and compressive loads in Fig. 13. Due to the limitations on the maximum displacement applied to the test setup, none of the specimens have reached their maximum loading capacity. In other words, the torsion failure of pipes will occur in higher displacements or higher number of load cycles, and thus ductility capacity of the damper can be larger than what is obtained in the figure.

4.2 Numerical results

Numerical analysis is done using finite element method in ABAQUS software (ABAQUS Inc. 2014). Pipes are modeled using 1100 three-dimensional twenty-node brick elements (C3D20) which have three degrees of freedom at each node. Other parts of the setup are modeled using 2350 two-dimensional eight-node shell elements (S8R5) which have five degrees of freedom at each node. Dimensions of the elements are obtained using a sensitivity analysis and are 15 millimeters for pipes. Von Mises yielding surface

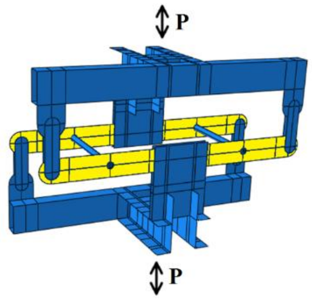

Fig. 14 Geometry of the numerical model and its loading

with a bilinear kinematic hardening is used for steel materials. A displacement control cyclic load is applied in FE model based on Fig. 12 loading protocol. Considering the significant effect of the deformation on the results, especially for displacements near the maximum displacement, in the numerical analysis of the dampers, geometric nonlinearity is considered.

Fig. 14 shows the geometry of the numerical model and the applied load on it. Also, Fig. 15 shows the meshing of the model and the stress distribution at the maximum displacement. As can be seen, the stress at any point in the pipe has exceeded the yielding limit. In Fig. 13, the load-displacement hysteretic behavior of numerical models for pipe 14, 21, 31 and 42 are compared with the experimental results. It can be seen that numerical models properly simulate experimental results. Of course, there are some differences between numerical and experimental results, mainly due to the idealizing assumptions in numerical models. Also, the higher manufacturing accuracy in pipe 14 results in better consistency between numerical and experimental results for this pipe compared to other pipes. The pipe fabrication errors consist of changes in the thickness of the pipe in different parts of it and imprecise circular section. These errors in pipes 21, 31 and 42 result

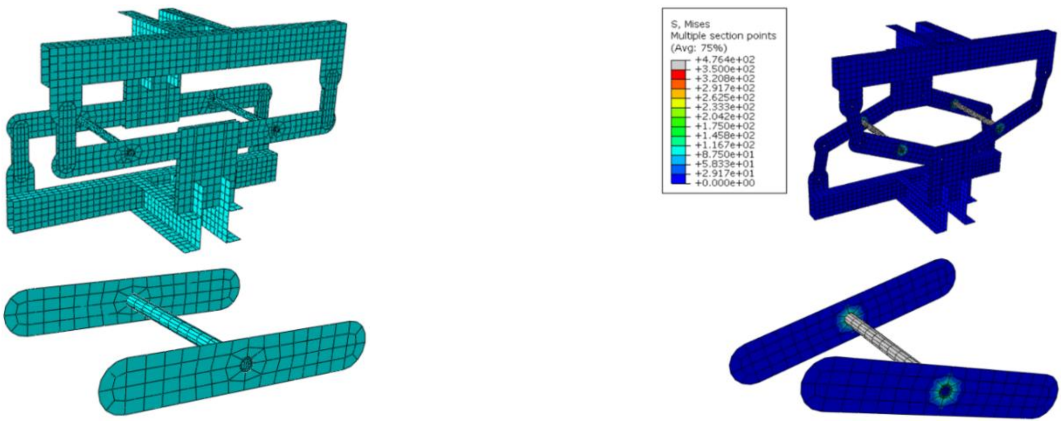

(a) Geometry of meshed modely (b) Stress distribution during loading

Fig. 15 Numerical model

in a significant difference between experimental and numerical results in the second and fourth quarters of hysteretic loops. Other sources of inconsistency between numerical and experimental results are experimental tolerances, such as the presence of clearance at connections, and setup fabrication errors.

4.3 Comparison of the results

In this section, characteristics of the proposed damper obtained from experimental testing, numerical analysis and analytical relationships are compared. Characteristics of dampers such as the initial stiffness, K_i, yielding force, P_y, yielding displacement, δ_y, energy amount dissipated in outer cycle of hysteretic behavior, E_{pl}, and ultimate exerted force in compression, P_{uc}, and tension, P_{ut}, are compared in Table 3. The beginning point of nonlinear behavior in the load-displacement curve is adopted as yield point to determine yielding force and displacement of the dampers. The yielding force and displacement of the specimens are obtained analytically using Eqs. (13) and (19), respectively. The ultimate force capacity of the specimens in compression and tension are calculated analytically using Eq. (21) for negative and positive displacements, respectively. Also, the analytical values of the initial stiffness and dissipated energy in the outmost loading loop of the specimens are calculated by use of Eqs. (20) and (24), respectively. Comparison between analytical, numerical and experimental results in Table 3 shows that analytical relationships results appropriately predict structural characteristics of the damper.

The initial stiffness and yielding force obtained from analytical, numerical and experimental results differ less than 16% and approximately are the same. Ignoring residual stresses created in production process of the pipes and simplifying assumptions in the analytical relationships and numerical analysis result in larger yielding displacement in experimental specimens. Results in Table 3 demonstrate

Table 3 Comparison of analytical, numerical and experimental results

Specimens		Specifications					
		Initial stiffness (K_i) (kN/mm)	Yield force (P_y) (kN)	Yield displacement (δ_y)	Dissipated energy (E_{pl}) (kJ)	P_{uc} (in compression) (kN)	P_{ut} (in tension) (kN)
Pipe14	Analytical	0.043	1.43	33.14	0.73	-1.72	2.00
	Experimental	0.037	1.28	34.60	0.62	-1.88	2.13
	Numerical	0.043	1.35	31.40	0.61	-1.80	2.10
Pipe21	Analytical	0.207	3.10	14.97	1.73	-3.60	4.17
	Experimental	0.189	2.95	15.60	1.43	-3.80	4.40
	Numerical	0.204	3.13	15.34	1.62	-3.72	4.33
Pipe31	Analytical	0.797	7.97	10.00	4.49	-8.82	10.23
	Experimental	0.761	7.40	9.73	3.70	-9.56	10.91
	Numerical	0.774	8.13	10.50	4.19	-9.28	10.78
Pipe42	Analytical	2.060	16.03	7.78	8.52	-17.21	19.97
	Experimental	1.880	14.72	7.83	7.78	-19.25	21.81
	Numerical	1.940	17.20	8.86	8.32	-18.98	22.06

that in spite of simplification applied in Eq. (24), dissipated energy in external loop of experimental samples are estimated properly. There is a good agreement between the ultimate forces of the damper in compression and tension attained from analytical, numerical and experimental results with differences up to 4% between numerical and experimental results and 10% between analytical and experimental results. Discarding strain hardening and assuming ideal elastic-perfectly plastic stress-strain curve for steel material decreases ultimate force obtained from analytical relationships in compare with numerical analysis which consider kinematic hardening for steel material.

5. Performance of the frame equipped with the proposed damper

The effect of proposed damper device on the performance of the steel structures is studied in this section. Therefore, the behavior of moment frames with/without the proposed damper during earthquake excitations is investigated by dynamic analysis.

5.1 The analytical model

Comparison between numerical and experimental results for the proposed damper in Table 3, shows that finite element method can be used to simulate the cyclic behavior of the proposed damper with a good accuracy. But, finite element simulation with shell/solid elements is not a practical method for real structures due to large number of degrees of freedom and high computation costs. Therefore, an analytical model of the proposed damper should be developed to consider the cyclic behavior of this device in the real structures equipped with the proposed damper.

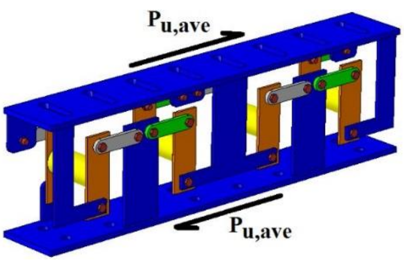

Fig. 16 Details of the proposed device to create symmetric behavior

The relationship of ultimate force capacity of the proposed damper in Eq. (21) is derived assuming ideal elastic-perfectly plastic stress-strain curve for steel material which underestimate the ultimate strength of the device as observed in Sec. 4.3. As shown in Fig. 8, the strength of the material increases after initial yielding point. An increasing factor, C_p, can be multiplied in Eq. (21) to consider strain hardening effects in the ultimate capacity of the damper device, as below

$$P_u' = C_p \frac{2n\pi(c_o^3 - c_i^3)\tau_y}{3R_0} \times \frac{\cos\alpha}{\cos(\alpha + j\frac{\phi}{2})} \tag{26}$$

where, P'_u is the modified ultimate force capacity of the damper device and C_p is a factor to consider the effect of strain hardening of material on the strength of the proposed device.

Comparing analytical and experimental results of the specimens in Table 3, demonstrate that the difference between analytical and experimental ultimate force capacity of the proposed device is less than 10%. Hence, this factor can be set as C_p = 1.1 in the analytical model of the proposed damper.

Large deformations lead to different ultimate strength in negative and positive displacements due to different rotation angle of the handle and link, as observable in Fig. 4. A symmetric behavior in positive and negative displacements can be achieved considering details demonstrated in Fig. 16. In this arrangement scheme, an even number of pipes in the damper device should be used. The links should be aligned in which the links located on the left and right side of the handle, alternatively. In this case, the ultimate capacity of the damper device, $P_{u,ave}$, is the same in positive and negative displacements and equals to average value of the tensile and compressive capacity, as below

$$P_{u,ave} = \frac{|P_{ut}'| + |P_{uc}'|}{2} \tag{27}$$

where, P'_{ut} and P'_{uc} are the modified ultimate tensile and compressive capacity of the proposed device, respectively, calculated by Eq. (26).

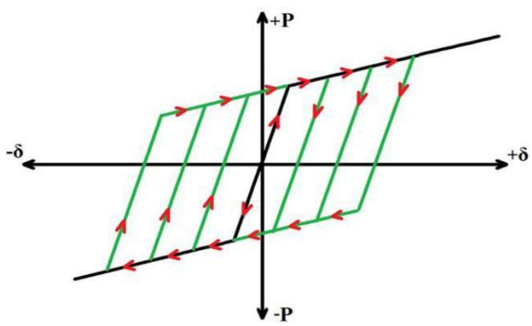

(a) Cyclic behavior

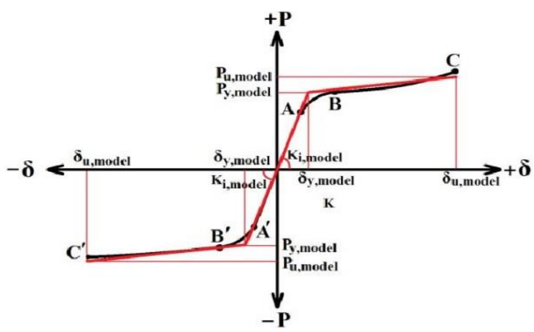

(b) Bilinear skeleton curve

Fig. 17 The analytical model

The cyclic load-displacement curve of the analytical model is illustrated in Fig. 17(a). A bilinear curve with kinematic hardening rule is adopted for the skeleton curve of the analytical model. The skeleton curve of the analytical model is compared with the monotonic load-displacement curve of the proposed damper in Fig. 17(b). In this figure, points A and A' are corresponding to yielding initiating at the outer wall of the pipe, P_y, as shown in Fig. 6(a), whereas points B and B' are corresponding to yielding at the inner wall of the pipe (see Fig. 6(c)). In Fig. 17(b), the ultimate force capacity of the damper in tension and compression are attained in point C and C', respectively. The analytical relationships derived in Sec. 3 with some modifications are used to obtain the characteristics of the analytical model, as below

$$K_{\mathrm{i,model}} = K_i \tag{28}$$

$$P_{\mathrm{y,model}} = P_{u0} \tag{29}$$

$$\delta_{\mathrm{y,model}} = \frac{P_{\mathrm{y.model}}}{K_{\mathrm{i,model}}} \tag{30}$$

$$P_{\mathrm{u,model}} = P_{\mathrm{u,ave}} \tag{31}$$

$$\delta_{\mathrm{u,model}} = \delta_{\mathrm{max,design}} \tag{32}$$

where, K_i is the initial stiffness of the proposed damper (Eq. (20)), P_{u0} is the force corresponding to yielding at the inner wall of the pipe and point B and B' in Fig. 17(b) (Eq. (14)), $P_{u,ave}$ is the ultimate capacity of the damper device with arrangement of Fig. 16 (Eq. (27)), and $\delta_{max,design}$ is the maximum bearable displacement which the damper is designed for it.

5.2 Studied frame

In order to investigate the behavior of structures equipped with the proposed damper, a study on the effect of proposed damper in steel structures is conducted. A five story-three bay moment frame belong to a five story building is considered for this study as illustrated in Fig. 18(a). The seismic base shear of the frame is calculated to be 331 kN using equivalent static method according to the Iranian Code of Practice for Seismic Resistant Design of Building (BHRC 2014). Accordingly, the story forces are obtained for this frame as shown in Table 4. The members of the frame are designed according to specifications of Iran's National Building Code for Steel Structures (INBC 2013) as demonstrated in Fig. 18(a). Effect of the proposed damper is investigated by adding the dampers to the assumed fame as illustrated in Fig. 18(b). The damper of each story is designed to tolerate story shear entirely due to higher stiffness of the inverted V brace used in the proposed system in compare with the moment frame. The properties of the designed dampers are shown in Table 4. The parameters of the analytical model of the damper device (see Fig. 17(b)) are demonstrated in Table 5 for dynamic analysis study.

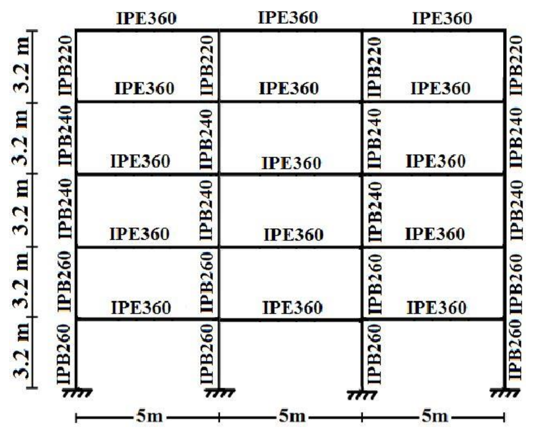

(a) Moment frame

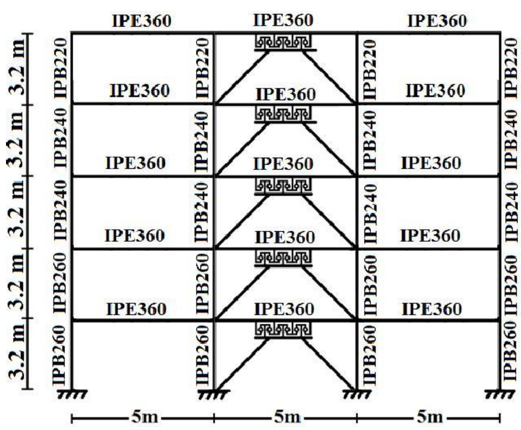

(b) Frame equipped with the proposed damper

Fig. 18 Assumed 5-story frames

Table 4 Properties of the damper devices

Story	Story force (kN)	Story shear (kN)	Steel type	Outer radius of the pipe (c_o) (mm)	Thickness (t) (mm)	Number of pipe	Length of the handle ($2R_0$) (mm)	Length of the pipe (L) (mm)	Damper capacity ($P_{u,ave}$) (kN)
5	113	113	St52	58	3	6	354	300	123
4	90	203	St52	58	6	6	354	300	221
3	66	269	St52	58	6	6	285	300	291
2	43	312	St52	62	6	6	285	300	337
1	20	332	St52	64	6	6	285	300	362

Table 5 Parameters of the analytical model

Story	$K_{i,model}$ (Eq. (28)) (kN/mm)	$P_{y,model}$ (Eq. (29)) (kN)	$\delta_{y,model}$ (Eq. (30)) (mm)	$P_{y,model}$ (Eq. (31)) (kN)	$\delta_{u,model}$ (Eq. (32)) (mm)
5	17.4	103.3	6.0	111.8	128
4	29.7	185.4	6.3	200.5	128
3	45.8	230.3	5.0	264.3	128
2	57.1	266.9	4.7	306.3	128
1	63.4	286.2	4.5	328.5	128

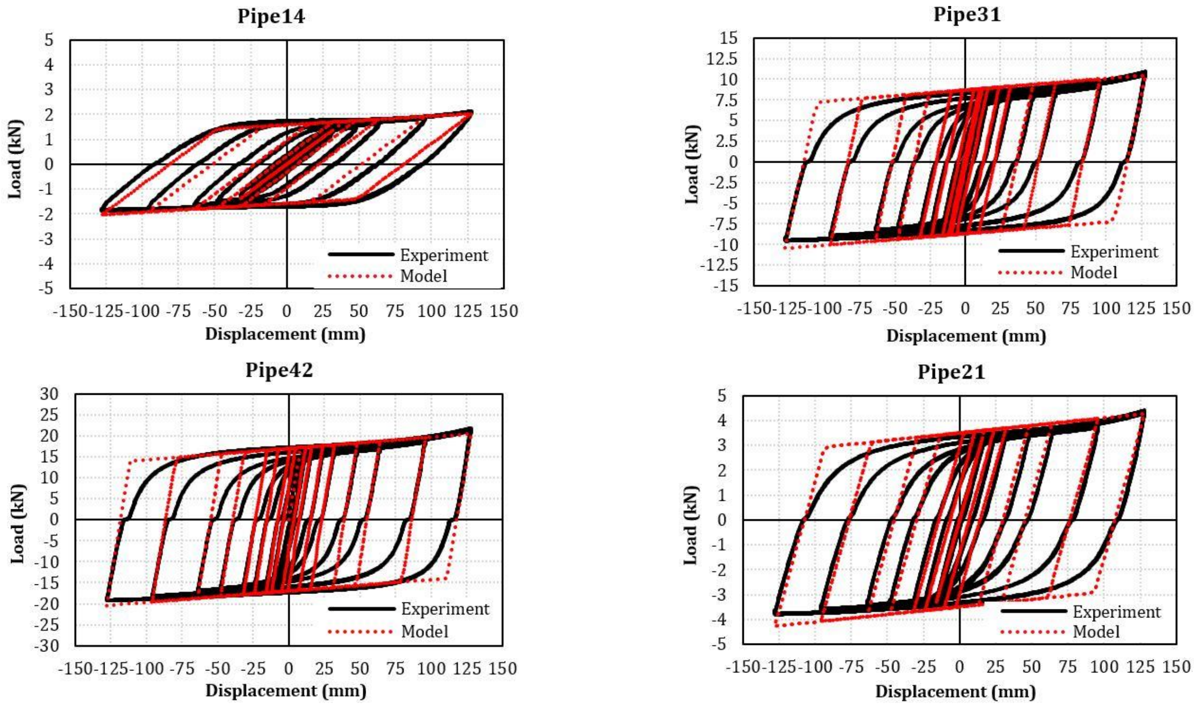

Fig. 19 Load-displacement hysteresis of the analytical model versus experimental results

5.3 Verification of the analytical model

The hysteresis of the analytical model for the tested specimens are compared with the experimental results in Fig. 19. The appropriate accuracy of the analytical model is observed in this figure.

In order to investigate the accuracy of the analytical model in simulating cyclic behavior of the proposed damper, results of the analytical model and finite element method is compared for a single story-one bay frame considering story beams and pin supports equipped with the proposed damper as illustrated in Fig. 20. The specifications of the damper device used in second and the fourth story of the studied frame (see Fig. 18(b) and Tables 4 and 5) were chosen to be verified. This verification has been performed using finite element method with ABAQUS software (ABAQUS Inc. 2014). About 3300 three-dimensional twenty-node brick elements (C3D20) and 10000 two-dimensional eight-node shell elements (S8R5) were respectively used for pipes and other parts of the FE model. Also, the loading protocol of the experimental study shown in Fig. 8 was used in this verification. Other considerations of the finite element model are the same as Section 4.2. The

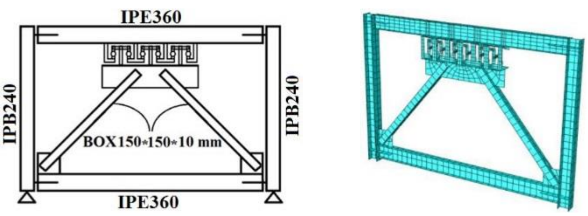

(a) Details (b) Finite element mesh

Fig. 20 Frame of the verification study equipped with the proposed damper

hysteresis of the analytical model and finite element model are compared in Fig. 21. This comparison shows that the analytical model can accurately be used to simulate cyclic behavior of the proposed damper in the analysis of structures equipped with the proposed damper.

5.4 Dynamic analysis and discussion

Effects of new device on the behavior of real structures are investigated in this section using dynamic analysis of an assuming frame (see Fig. 18) with/without damper under

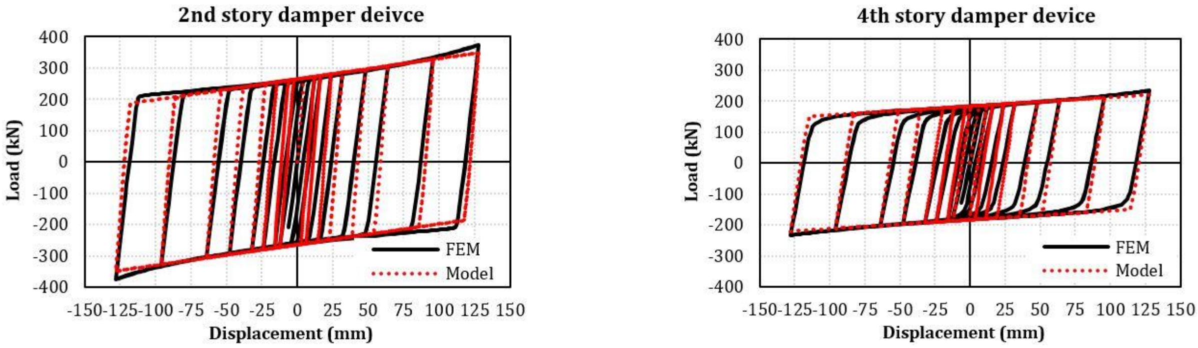

(a) Frame equipped with the second story damper

(b) Frame equipped with the fourth story damper

Fig. 21 The results of the analytical model versus finite element analysis

Table 6 Description of the ground motions used in this study (Riahi and Estekanchi 2010)

Date	Earthquake Name	Magnitude (Ms)	Station Number	Component (deg)	PGA (cm/s^2)	Abbreviation
06/28/92	Landers	7.5	12149	0	167.8	LADSP000
10/17/89	Loma Prieta	7.1	58065	0	494.5	LPSTG000
10/17/89	Loma Prieta	7.1	47006	67	349.1	LPGIL067
10/17/89	Loma Prieta	7.1	58135	360	433.1	LPLOB000
10/17/89	Loma Prieta	7.1	1652	270	239.4	LPAND270
04/24/84	Morgan Hill	6.1	57383	90	280.4	MHG06090
01/17/94	Northridge	6.8	24278	360	504.2	NRORR360

Table 7 Story drift (W = with damper; W/O = without damper)

Story	LADSP000		LPSTG000		LPGIL067		LPLOB000		LPAND270		MHG06090		NRORR260		Average	
	W/O	W	W/O	W	W/O	W	W/O	W	W/O	W	W/O	W	W/O	W	W/O	W
5	1.20	0.49	1.63	0.73	1.17	0.99	2.17	0.54	1.41	0.86	1.84	0.83	1.65	0.94	1.58	0.77
4	1.82	0.69	2.55	1.13	1.09	0.98	2.55	0.79	1.84	1.35	2.61	1.37	2.43	1.51	2.13	1.12
3	2.51	0.84	3.60	1.50	2.23	1.00	2.78	1.22	2.12	1.80	3.56	2.00	3.11	2.15	2.84	1.50
2	2.61	0.94	3.58	1.45	2.65	1.10	3.13	1.40	1.95	1.75	3.50	2.13	2.96	2.40	2.91	1.60
1	1.87	0.71	2.52	1.02	2.25	0.76	2.39	1.05	1.33	1.23	2.40	1.62	2.00	1.89	2.11	1.18
Max.	2.61	0.94	3.60	1.50	2.65	1.10	3.13	1.40	2.12	1.80	3.56	2.13	3.11	2.40	2.97	1.61
Difference (%)	64.0		58.3		58.5		55.3		15.1		40.2		22.8		45.8	

earthquake excitation. Seven earthquake records have been used in dynamic analysis of the frame. The specifications of these earthquake records are visible in Table 6. A dynamic time-history analysis has been performed in accordance with the procedure explained in work of Riahi and Estekanchi (Riahi and Estekanchi 2010). The maximum story drift of the moment frame with/without damper is plotted in Fig. 22 for each earthquake record. The values of maximum story drift can be compared for various story/record in Table 7. This comparison demonstrates that, equipping moment frame with the proposed damper device reduces the maximum story drift of the frame between 15% and 60% with an average about 50% in compare with initial moment frame without damper for all earthquake records. Also, the maximum base shear of the frame with/without damper device is obtained in dynamic analysis and compared in Table 8. As shown in this table, using the proposed damper device in the moment frame has a varying effect on the maximum base shear of the moment frame due to different characteristics of the earthquake records including time duration, frequency contents, and peak ground acceleration (PGA). However, this study showed that, the proposed damper reduces the value of maximum base shear of the moment frame approximately 5% in average.

6. Conclusions

In this paper, a new type of yielding damper with pipe

Table 8 Maximum Base Shear (W = with damper; W/O = without damper)

Story	LADSP000	LPSTG000	LPGIL067	LPLOB000	LPAND270	MHG06090	NRORR260	Average
W	1005.9	1198.0	1275.2	1332.6	746.4	1149.3	1064.4	1110.3
W/O	748.2	940.1	822.1	1040.9	1081.5	1263.2	1408.5	1043.5
Difference (%)	25.6	21.5	35.5	21.9	-44.9	-9.9	-32.3	6.0

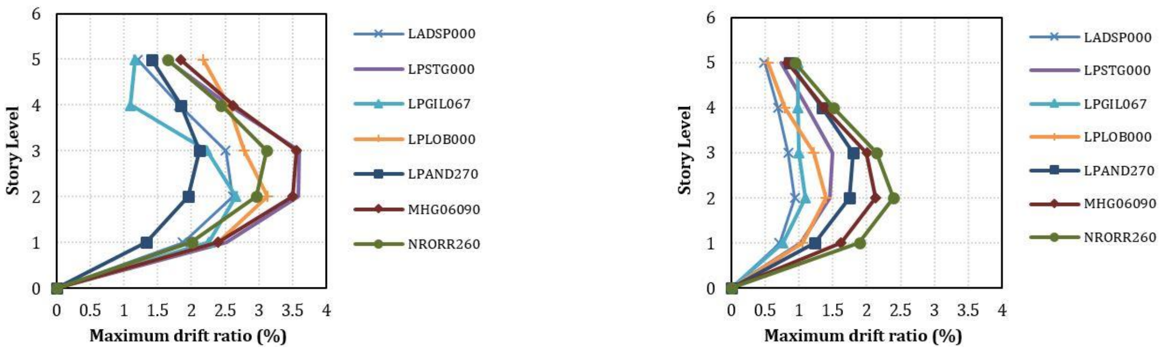

(a) Moment frame (b) Moment frame equipped with damper

Fig. 22 Maximum inter-story drift ratios (%) obtained by time history dynamic analysis

section which works under pure torsion is introduced. Using a special loading mechanism, pure torsion is created in the ductile part of the damper. Therefore, a uniform-distributed shear stress is caused in the pipe wall due to pure torsion and therefore it is possible to use a large amount of energy dissipating capacity of the damper material. First, analytical relationships governing the damper behavior are extracted assuming elastic perfectly plastic behavior for material. Then, four experimental specimens of the damper are tested and also their numerical models are studied. The structural characteristics of the proposed damper, including the initial stiffness, yielding force, yielding displacement, energy amount dissipated in a cycle of hysteretic behavior, and ultimate force of the dampers derived from analytical relationships, experimental results, and numerical analysis are compared. An analytical model based on theoretical relationships is developed and verified using test results. This model can be used in the dynamic analysis to simulate the cyclic behavior of the proposed damper in the frames equipped with the proposed damper. A numerical study on the performance of the frames equipped with the proposed damper is conducted. The performance of a five story- three bay moment frame with/without proposed damper is studied using dynamic analysis for seven earthquake records. The summary of the results of this research is as follows:

- Based on the analytical relationships presented, it can be concluded that shear force capacity, energy dissipation capacity and ductility of the dampers depend on the diameter and material type of the pipe and the length of handle connected to the pipe. Increasing torsional capacity of the pipe, by changing its material, diameter and thickness, leads to an increase in shear force capacity and energy dissipation capacity of the damper. Increasing the length of the pipes and the length of the handles, as well as the use of materials with higher ductility for the pipes, increase ductility capacity of the damper. Therefore, for a desirable structural performance and required strength and ductility, a suitable damper can be designed and used in the structure.
- Experimental results indicate the consistent and stable behavior of the proposed damper under cyclic loading. The hysteretic behavior of the damper shows suitable ductility and there is no stiffness reduction and strength degradation in it. The damper shows this performance even at a displacement of 128 mm, corresponding to a story drift of 4% for conventional structures. Nonlinear and asymmetric behavior of damper force-displacement at large deformations in experimental results are due to the asymmetric decrease in the effective arm of the torsion applied to the pipes in tensile and compressive force. This reduction increases the shear force of the damper in large deformations. No failure is found in experimental results and there is no significant change in the hysteretic behavior of the damper and therefore it can be predicted that the ductility capacity of the damper is greater than the values obtained in the test.
- The results of numerical analysis using finite element method indicate their proper ability to simulate the actual performance of the damper under cyclic loads. In other words, using ideal and simplifying assumptions in numerical modeling does not lead to a significant error in the results. Also, these results clearly show that when the damper reaches its maximum displacement, all parts of the pipe have experienced yielding. This issue confirms the proper performance of the damper in developing pure torsion in the pipe.
- Comparison of the results of the analytical relationships presented in this paper with the results of numerical analysis and experimental modeling

indicates the acceptable accuracy of these relationships in estimating characteristics of the damper. The difference between the results are due to the use of ideal and simplifying assumptions in these relationships, as well as pipe and setup manufacturing errors, and the difference is in acceptable range. These analytical relationships can be used to design structures equipped with the proposed damper.

- The dynamic analysis of the moment frame with/without proposed damper demonstrate that the proposed damper device reduces maximum story drift of the frames in all of cases. This reduction is between 15% and 60% for different earthquakes with an average of 46%. The proposed device decreases maximum base shear of the frames during earthquake in some of cases. The average of maximum base shear of the structures equipped with the proposed damper under different earthquakes shows about 5% reduction in compare with the initial moment frame without dampers.

References

ABAQUS Inc. (2014), ABAQUS/Theory User Manual, Version 6.14, USA.

Abebe, D.Y. and Choi, J.H. (2014), "Analytical study on hysteretic characteristics of circular shear panel damper", *Proceeding of International Conference on Advances in Civil, Structural and Mechanical Engineering*, London, UK.

Aguirre, M. and Sanchez, A.R. (1992), "Structural seismic damper", *ASCE J. Struct. Eng.*, **118**(5), 1158-1171. https://doi.org/10.1061/(ASCE)0733-9445(1992)118:5(1158)

Benavent-Climent, A. (2010), "A brace-type seismic damper based on yielding the walls of hollow structural sections", *Eng. Struct.*, **32**, 1113-1122. https://doi.org/10.1016/j.engstruct.2009.12.037

BHRC (2014), Iranian Code of Practice for Seismic Resistant Design of Buildings, Standard No 2800; Building and Housing Research Centre, Tehran, Iran. [In Persian]

Black, C., Makris, N. and Aiken, I. (2004), "Component testing, seismic evaluation and characterization of buckling-restrained braces", *ASCE J. Struct. Eng.*, **130**, 880-894. https://doi.org/10.1061/(ASCE)0733-9445(2004)130:6(880)

Chan, R.W.K. and Albermani, F. (2008), "Experimental study of steel slit damper for passive energy dissipation", *Eng. Struct.*, **30**(4), 1058-1066. https://doi.org/10.1016/j.engstruct.2007.07.005

Chan, R.W.K., Albermani, F. and Kitipornchai, S. (2013), "Experimental study of perforated yielding shear panel device for passive energy dissipation", *J. Constr. Steel Res.*, **91**, 14-25. https://doi.org/10.1016/j.jcsr.2013.08.013

Cheraghi, A. and Zahrai, S.M. (2017), "Cyclic testing of multi-level pipe in pipe damper", *J. Earthq. Eng.*, **23**(10), 1695-1718. https://doi.org/10.1080/13632469.2017.1387191

Ciampi, V. and Marioni, A. (1991), "New types of energy dissipating devices for seismic protection of bridges", *Proceeding for 3rd World Congress on Joint Sealing and Bearing Systems for Concrete Structures,* New York, USA.

Deng, K., Pan, P. and Wang, C. (2013), "Development of crawler steel damper for bridges", *J. Constr. Steel Res.*, **85**, 140-150. https://doi.org/10.1016/j.jcsr.2013.03.009

Deng, K., Pan, P., Li, W. and Xue, Y. (2015a), "Development of a buckling restrained shear panel damper", *J. Constr. Steel Res.*, **106**, 311-321. https://doi.org/10.1016/j.jcsr.2015.01.004

Deng, K., Pan, P., Su, Y. and Xue, Y. (2015b), "Shape optimization of U-shaped damper for improving its bi-directional performance under cyclic loading", *Eng. Struct.*, **93**, 27-35. https://doi.org/10.1016/j.engstruct.2015.03.006

Farzampour, A., Eatherton, M.R., Mansouri, I. and Hu, J.W. (2019), "Effect of flexural and shear stresses simultaneously for optimized design of butterfly-shaped dampers: computational study", *Smart Struct. Syst., Int. J.*, **23**(4), 329-335. http://dx.doi.org/10.12989/sss.2019.23.4.32

Franco, J.M., Cahís, X., Gracia, L. and López, F. (2010), "Experimental testing of a new anti-seismic dissipator energy device based on the plasticity of metals", *Eng. Struct.*, **32**(9), 2672-2682. https://doi.org/10.1016/j.engstruct.2010.04.037.

Gray, M., Christopoulos, C., Packer, J. and De Oliveira, C. (2012), "A new brace option for ductile braced frames", *Mod. Steel Constr.*, **52**(2), 40-43.

Hitaka, T. and Matsui, C. (2003), "Experimental study on steel shear wall with slits", *ASCE J. Struct. Eng.*, **129**, 586-595. https://doi.org/10.1061/(ASCE)0733-9445(2003)129:5(586)

INBC (2013), Iranian national building code, part 10, Design and Construction of Steel Structures; Ministry of Housing and Urban Development, Tehran, Iran. [In Persian]

Kato, S. and Kim, Y.B. (2006), "A finite element parametric study on the mechanical properties of J-shaped steel hysteresis devices", *J. Constr. Steel Res.*, **62**(8), 802-811. https://doi.org/10.1016/j.jcsr.2005.11.014

Kato, S., Kim, Y.B., Nakazawa, S. and Ohya, T. (2005), "Simulation of the cyclic behavior of J-shaped steel hysteresis devices and study on the efficiency for reducing earthquake responses of space structures", *J. Constr. Steel Res.*, **61**(10), 1457-1473. https://doi.org/10.1016/j.jcsr.2005.03.006

Lee, C.H., Ju, Y.K., Min, J.K., Lho, S.H. and Kim, S.D. (2015), "Non-uniform steel strip dampers subjected to cyclic loadings", *Eng. Struct.*, **99**, 192-204. https://doi.org/10.1016/j.engstruct.2015.04.052

Milani, A.S. and Dicleli, M. (2016), "Systematic development of a new hysteretic damper based on torsional yielding: part I—design and development", *Earthq. Eng. Struct. Dyn.*, **45**(6), 845-867. https://doi.org/10.1002/eqe.2684

Milani, A.S. and Dicleli, M. (2017), "Low-cycle fatigue performance of solid cylindrical steel components subjected to torsion at very large strains", *J. Constr. Steel Res.*, **129**, 12-27. https://doi.org/10.1016/j.jcsr.2016.10.019

Nakashima, M., Iwai, S., Iwata, M., Takeuchi, T., Konomi, S., Akazawa, T. and Saburi, K. (1994), "Energy dissipation behaviour of shear panels made of low yield steel", *Earthq. Eng. Struct. Dyn.*, **23**(12), 1299-1313. https://doi.org/10.1002/eqe.4290231203

Piedrafita, D., Cahis, X., Simon, E. and Comas, J. (2013), "A new modular buckling restrained brace for seismic resistant buildings", *Eng. Struct.*, **56**, 1967-1975. https://doi.org/10.1016/j.engstruct.2013.08.013

Piedrafita, D., Cahis, X., Simon, E. and Comas, J. (2015), "A new perforated core buckling restrained brace", *Eng. Struct.*, **85**, 118-126. https://doi.org/10.1016/j.engstruct.2014.12.020

Razavi, S.A., Mirghaderi, S.R. and Hosseini, A. (2014), "Experimental and numerical developing of reduced length buckling-restrained braces", *Eng. Struct.*, **77**, 143-160. https://doi.org/10.1016/j.engstruct.2014.07.034

Riahi, H.T. and Estekanchi, H.E. (2010), "Seismic assessment of steel frames with the endurance time method", *J. Constr. Steel Res.*, **66**, 780-792. https://doi.org/10.1016/j.jcsr.2009.12.001

Shih, M.H. and Sung, W.P. (2005), "A model for hysteretic behavior of rhombic low yield strength steel added damping and stiffness", *Comput. Struct.*, **83**(12), 895-908. https://doi.org/10.1016/j.compstruc.2004.11.012

Skinner, R.I., Kelly, J.M. and Heine, A.J. (1975), "Hysteretic dampers for earthquake-resistant structures", *Earthq. Eng. Struct. Dyn.*, **3**(3), 287-296. https://doi.org/10.1002/eqe.4290030307

Tagawa, H. and Gao, J. (2012), "Evaluation of vibration control system with U-dampers based on quasi-linear motion mechanism", *J. Constr. Steel Res.*, **70**, 213-225. https://doi.org/10.1016/j.jcsr.2011.09.004

Tsai, K.C., Chen, H.W., Hong, C.P. and Su, Y.F. (1993), "Design of steel triangular plate energy absorbers for seismic-resistant construction", *Earthq. Spectra*, **9**(3), 505-528. https://doi.org/10.1193/1.1585727

Tsopelas, P. and Constantinou, M.C. (1997), "Study of elastoplastic bridge seismic isolation system", *J. Struct. Eng.*, **123**(4), 489-498. https://doi.org/10.1061/(ASCE)0733-9445(1997)123:4(489)

Vetr, M.G. and Ghamari, A. (2012), "Improving of seismic performance of steel structures using an innovative passive energy damper with torsional mechanism", *Int. J. Civil Environ. Eng.*, **12**(5), 63-69.

Whittaker, A., Bertero, V., Alonso, J. and Thompson, C. (1989), "Earthquake simulator testing of steel plate added damping and stiffness elements", Report No. UCB/EERC-89/02; Earthquake Engineering Research Center, University of California, Berkeley, CA, USA.

Zahrai, S.M. and Mortezagholi, M.H. (2017), "Cyclic performance of an elliptical-shaped damper with shear diaphragms in chevron braced steel frames", *J. Earthq. Eng.*, **22**(7), 1209-1232. https://doi.org/10.1080/13632469.2016.1277436

Zibasokhan, H., Behnamfar, F. and Azhari, M. (2019), "Experimental study of a new pure bending yielding dissipater", *Bull. Earthq. Eng.*, **17**(7), 4389-4410. https://doi.org/10.1007/s10518-019-00616-1

FC